Journal of Power Sources 196 (2011) 2005–2012

Contents lists available at ScienceDirect

Journal of Power Sources

journal homepage: www.elsevier.com/locate/jpowsour

High-temperature tensile and creep properties of a ferritic stainless steel for interconnect in solid oxide fuel cell

Yung-Tang Chiu, Chih-Kuang Lin*, Jiunn-Chi Wu

Department of Mechanical Engineering, National Central University, 300 Jhong-Da Rd., Jhong-Li 32001, Taiwan

ARTICLE INFO

Article history:
Received 5 August 2010
Received in revised form
24 September 2010
Accepted 24 September 2010
Available online 23 October 2010

Keywords:
Planar solid oxide fuel cell
Ferritic stainless steel
High temperature
Creep properties
Tensile properties

ABSTRACT

The purpose of this study is to investigate the high-temperature mechanical properties of a ferritic stainless steel (Crofer 22 APU) for use as an interconnect material in planar solid oxide fuel cells (pSOFCs). Tensile properties of the Crofer 22 APU steel are evaluated at temperatures of 25–800 °C. Creep properties are evaluated by constant-load tests at 650–800 °C. Several creep lifetime models are applied to correlate the creep rupture time with applied stress or minimum creep rate. Experimental results show the variation of yield strength with temperature can be described by a sigmoidal curve for different deformation mechanisms. The creep stress exponent, n, has a value of 5 or 6, indicating a power-law creep mechanism involving dislocation motion. The apparent activation energy for such a power-law creep mechanism is estimated as 393 kJ mol^{-1} through some thermally activated relations. Creep rupture time of the Crofer 22 APU steel can be described by a Monkman–Grant relation with a time exponent, $m = 1.11$. The relation between creep rupture time and normalized stress is well fitted by a universal simple power law for all of the given testing temperatures. Larson–Miller relationship is also applied and shows good results in correlating the creep rupture time with applied stress and temperature for the Crofer 22 APU steel. Fractographic and microstructural observations indicate most of the creep cavities are nucleated along grain boundaries and a greater amount of cavities are formed under high stresses.

1. Introduction

In recent development of planar solid oxide fuel cells (pSOFCs), an intermediate operation temperature between 600 and 800 °C is favorable to reduce system cost and enhance long-term stability [1]. A typical unit cell in a pSOFC stack is composed of a positive electrode-electrolyte-negative electrode (PEN) assembly plate, a supporting window frame, a porous nickel mesh, two interconnects, and gas seals. The interconnect in a pSOFC stack must have good electrical conductivity, low permeability of oxygen and hydrogen, suitable thermal conductivity, good chemical stability, adequate mechanical strength and creep resistance, and a good match in coefficient of thermal expansion (CTE) with other cell components. In addition, a cost-effective manufacture of a pSOFC stack requires an easy fabrication of interconnects [2]. As the operating temperature of pSOFCs is below 800 °C, it is possible to use metallic interconnects in replacement of the expensive ceramic interconnects [2–5]. Chromium-based and iron-based alloys are favorable for use as interconnects in pSOFC stacks. As compared to chromium-based alloys, iron-based alloys are more attractive due to their high ductility, good workability and low cost [2]. Among the iron-based alloys, Cr-rich ferritic stainless steels are considered as leading candidates for the interconnect in pSOFC stacks [2,6–10]. A major issue of ferritic stainless steels used in pSOFCs is their creep resistance at the high operating temperatures [11]. Creep resistance of the interconnect with a very small thickness is one of the important factors for a stable long-term operation of a pSOFC system [12].

The major sources of thermal stress in a pSOFC stack include mismatch of CTE and thermal gradient [13,14]. Under thermal cycling between steady-operation and shutdown stages, even a small CTE mismatch may give rise to significant thermal stresses in a pSOFC stack [13,14]. Therefore, thermal stress and structural integrity should not be neglected for design of a pSOFC system. Although the stresses induced by CTE mismatch may not result in failure of the interconnects immediately, it may generate creep deformation in the interconnects at a long-term high-temperature environment. The creep damage may eventually make metallic interconnects deform excessively and even generate cracks. The gas leakage due to such cracks would degrade the cell performance and efficiency. Therefore, a comprehensive creep analysis of the metallic interconnect is necessary for evaluating the structural durability of a pSOFC system.

For those metallic interconnects developed for pSOFC, their characteristics such as electrical conductivity, corrosion resistance, oxidation resistance, thermal properties, Cr evaporation, and long-

* Corresponding author. Tel.: +886 3 426 7340; fax: +886 3 425 4501.
E-mail address: t330014@cc.ncu.edu.tw (C.-K. Lin).

0378-7753/$ – see front matter © 2010 Elsevier B.V. All rights reserved.
doi:10.1016/j.jpowsour.2010.09.083

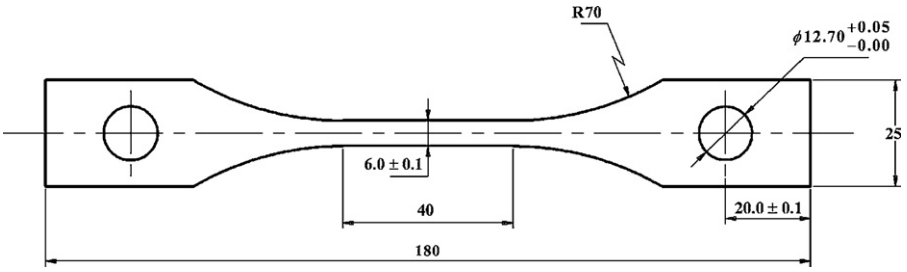

Fig. 1. Geometry of tensile and creep specimen with a thickness of 2.5 mm (dimensions in mm).

term stability have been widely investigated [4,6,15–18]. However, there is little work focused on the high-temperature mechanical properties of the metallic interconnect in the literature [11]. Therefore, it is still needed to study this issue so as to provide necessary information for design of a reliable pSOFC system. The high-temperature mechanical properties of a commercial ferritic stainless steel, Crofer 22 APU, developed for the interconnect in pSOFC are studied in the present work. In particular, the variation of tensile and creep properties with temperature are investigated for the given steel by systematic tests.

2. Experimental procedures

2.1. Material and specimen

The commercially available Crofer 22 APU ferritic stainless steel used in the current study was supplied by the vendor in the form of cold-rolled, annealed plates with a thickness of 2.5 mm. The chemical composition of this steel is listed in Table 1. From these plates, pin-loaded specimens were made in accordance with ASTM Standard E8 [19] for high-temperature tensile and creep tests. Geometry of the specimen is shown in Fig. 1. No further heat treatment was conducted on the specimens after machining.

2.2. Tensile test

Uniaxial tensile tests were conducted on a commercial closed-loop servo-hydraulic testing machine equipped with a furnace. The tensile tests were performed in air under displacement control with a stroke rate of 2 mm min^{-1}. The testing temperatures were set at 25, 300, 400, 500, 600, 650, 700, 750, and 800 °C to simulate the operating temperature range of pSOFCs. Each tested specimen was firstly held at the specified temperature for 15 min prior to applying the load. A commercial high-temperature axial extensometer with a 12-mm gauge length was used to measure the strain. When the strain value reached the upper limit (20%) of the extensometer, the extensometer was removed from the furnace and the tensile test was continued without measuring the strain until fracture of specimen. The final elongation was determined by putting back together the two broken pieces of the specimen and measuring the distance change between the two original gauge marks. The 0.2% offset yield strength S_y and ultimate tensile strength S_{UTS} were determined from the obtained engineering stress–strain curves.

2.3. Creep test

Creep tests were conducted in two ways. For high-stress, short-life tests, the creep tests were performed under constant load using the aforementioned, tensile testing equipment. The elongation of specimen was continuously monitored by the aforementioned high-temperature axial extensometer. For low-stress, long-life tests, a direct-load creep test machine was used to perform the constant-load creep tests. Various weights were used as the loading source in the direct-load creep test machine. The stress level can be adjusted by changing the weights applied. In this part of creep test, the elongation of specimen was monitored by periodic measurements of the distance change between two marked points with an initial gauge length of 12 mm. Note that each length measurement was taken after cooling down the specimen to room temperature. After each measurement, the specimen was heated up to the specified temperature again for another period of creep loading. The creep test lasting longer than 100 h was classified as a long-life test. Temperatures for creep test were set at 650, 700, 750, and 800 °C. Similar to the tensile test, each specimen was held at the specified temperature for 15 min prior to applying the load. The creep strain–time and stress–rupture time curves were then obtained from these tests.

2.4. Microstructural and fractographic analyses

After the tensile and creep tests, fracture surfaces of the specimens were observed with scanning electron microscopy (SEM). In addition, some of the tensile and creep specimens were cut perpendicularly to the loading axis, ground, and polished for metallographic preparation and observation. The microstructural change and creep damages were then observed and analyzed with SEM. The related precipitates in the microstructure were identified by energy dispersive spectrometry (EDS).

3. Results and discussion

3.1. Effect of temperature on tensile strength

Engineering stress–strain curves of Crofer 22 APU tested at different temperatures are shown in Fig. 2. Note only the strain less

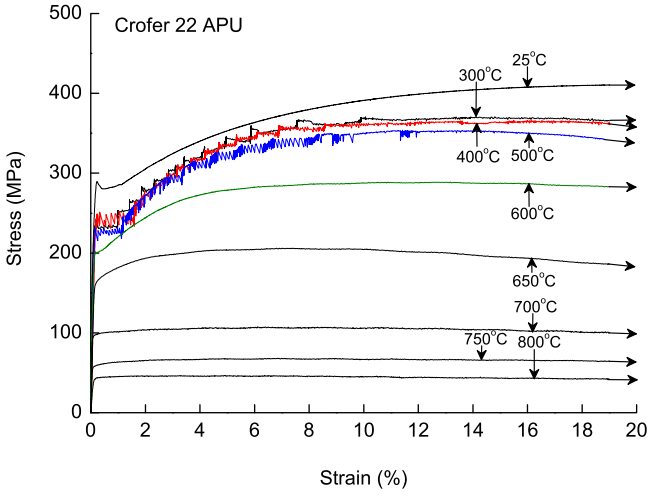

Fig. 2. Engineering stress–strain curves of Crofer 22 APU at different temperatures in the range of strain less than 20%.

Table 1
Chemical composition of Crofer 22 APU stainless steel tested (wt.%).

Fe	C	Cr	Mn	Si	Ti	Cu	S	P	Al	La
Bal.	0.003	22.71	0.44	0.02	0.07	0.01	<0.002	0.004	0.01	0.09

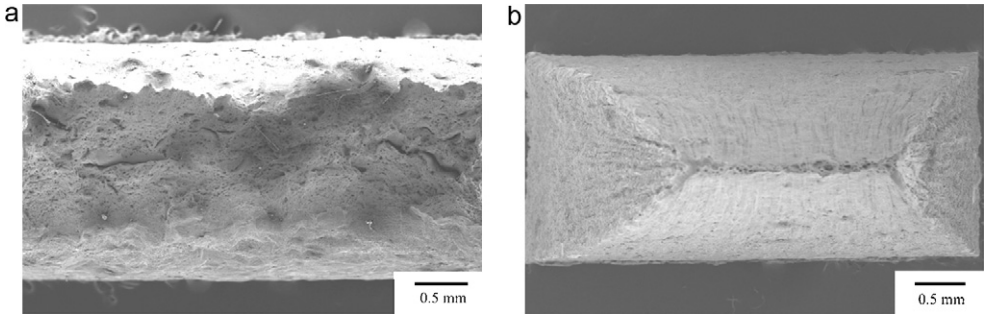

Fig. 3. Tensile fracture surfaces of Crofer 22 APU specimens tested at (a) 25 °C and (b) 700 °C.

than 20% is presented in Fig. 2, as the upper limit of the high-temperature extensometer is 20%. As shown in Fig. 2, the curves of 300, 400, and 500 °C show a typical dynamic strain aging (DSA) feature with serrated flows. The serrations could be attributed to an interaction of dislocations with solute atoms [20,21]. Table 2 shows the tensile properties of Crofer 22 APU at various temperatures. As shown in Table 2, the ultimate tensile strength and Young's modulus are decreased with increasing temperature. The yield strength is also generally decreased with an increase in temperature except at the temperature region of 300–500 °C. The yield strength has no significant change at 300–500 °C. A significant drop of tensile strength was observed between 650 and 700 °C with a reduction of 43% in yield strength. Fig. 3 shows the representative fractographs of tensile specimens fractured at 25 and 700 °C. The dimple features in Fig. 3 indicate a ductile fracture mode at both temperatures. A greater extent of reduction of cross-sectional area was observed at 700 °C due to high temperature softening.

A unified equation has been proposed by Chen et al. [22,23] to describe the variation of yield strength with temperature between room temperature and 1000 °C for some steels. This equation is described as follows:

$$\frac{S_{y,T}}{S_{y,25}} = a - \frac{(T-b)^n}{c} \quad (1)$$

where $S_{y,T}$ is the yield strength at temperature T °C, $S_{y,25}$ is the yield strength at room temperature (25 °C), and values of the coefficients a, b, c, and n are determined from fitting curves. This equation was applied to describe the temperature-dependent trend of yield strength in the current study. Values of the coefficients in Eq. (1) for Crofer 22 APU are obtained through curve fitting of the yield strength data. These values are presented in Table 3 with a separation of temperature into three regions. As shown in Fig. 4, the test results for the given Crofer 22 APU steel are well correlated by the proposed equation. The yield strength in the first region is slightly decreased with increasing temperature according to the fitted curve in Fig. 4. In addition to a high-temperature softening effect, there is also a hardening effect due to DSA at this temperature range. Therefore, the slight change in yield strength from 300 to 500 °C can be regarded as an interaction between the high-temperature softening and the DSA effects [24]. At the temperature region of 500–700 °C, the high-temperature softening effect dominated the mechanical behavior, as the yield strength is significantly decreased with increasing temperature. However, the yield strength in the third region of temperature above 700 °C is gradually decreased with increasing temperature again. This is pre-

Table 2
Tensile properties of Crofer 22 APU at various temperatures.

Temperature (°C)	Yield strength (MPa)	Ultimate tensile strength (MPa)	Young's modulus (GPa)	Elongation (in 12 mm) (%)
25	291	417	214	29
300	231	384	210	33
400	238	368	184	34
500	225	354	196	35
600	201	279	162	39
650	162	203	157	46
700	92	102	91	58
750	57	64	66	80
800	44	48	44	99

Table 3
Coefficients of the unified equation for Crofer 22 APU.

Temperature (°C)	a	b	c	n
$25 \le T < 500$	0.994	25.0	128	0.546
$500 \le T < 700$	0.774	449	2.47×10^8	3.35
$700 \le T < 800$	0.425	697	12.8	0.270

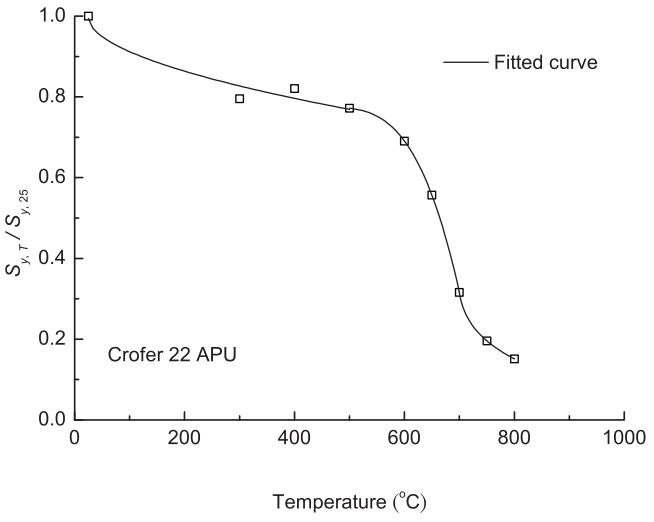

Fig. 4. Reduction factor of the yield strength of Crofer 22 APU at various temperatures.

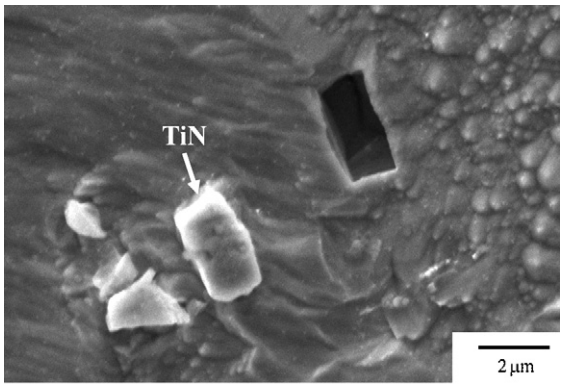

Fig. 5. SEM micrograph of typical precipitates of TiN in a Crofer 22 APU specimen after tensile test at 750 °C.

sumably due to a dynamic precipitation strengthening effect [25]. Tetragonal precipitates of TiN could be formed at high temperature in ferritic stainless steels with an addition of alloying element Ti [26]. A number of tetragonal precipitates, identified as TiN by EDS, were indeed found in the specimens after tensile test at 700 °C and above, as shown in Fig. 5. Therefore, the gradual decrease in yield strength with increasing temperature at temperature above 700 °C is related to an interaction between the high-temperature softening and the dynamic precipitation strengthening effects.

3.2. Creep behavior

Fig. 6 shows the typical creep strain curves for Crofer 22 APU at various temperatures. As shown in Fig. 6, the creep curves at all the given temperatures have a very short period of primary creep. This means that the strain hardening effect was rapidly recovered to make the creep strain increase at a constant rate soon after the load was applied. As also shown in Fig. 6, a larger applied stress caused a shorter rupture time at a given temperature.

The minimum strain rate for each creep curve in Fig. 6 was determined and plotted as a function of applied stress in Fig. 7. The following Norton's power law [27] was used to correlate the minimum strain rate with applied stress at a given temperature:

$$\dot{\varepsilon}_{\min} = f(T)\sigma^n \tag{2}$$

where $\dot{\varepsilon}_{\min}$ is the minimum creep strain rate, $f(T)$ is a temperature-dependent function, σ is the applied stress, and n is the stress exponent. In Fig. 7, the slope (n value) of each fitted straight line was determined according to Eq. (2). As shown in Fig. 7, the minimum creep strain rate is increased with applied stress at 650–800 °C, following the power-law relation. The value of stress exponent has been recognized as an index of creep deformation mechanism. A value of n in the range of 3–8 represents a dislocation type of creep mechanism [28]. In the current study, n has a value of about 5 at 650 and 700 °C and about 6 at 750 and 800 °C, corresponding to a power-law dislocation creep mechanism.

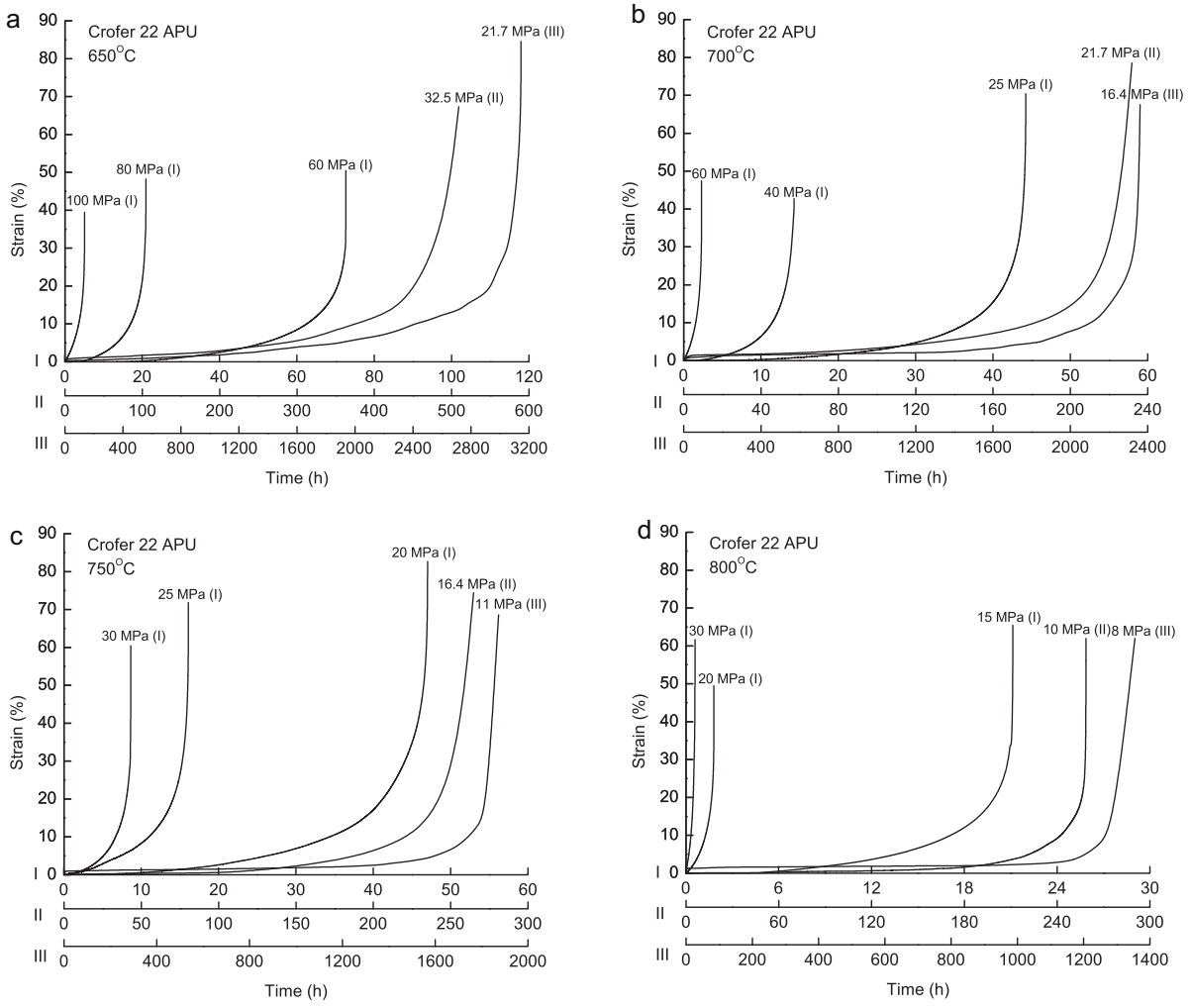

Fig. 6. Typical creep curves for Crofer 22 APU at various temperatures: (a) 650 °C, (b) 700 °C, (c) 750 °C, and (d) 800 °C (note that two or three scales are used in the abscissa)

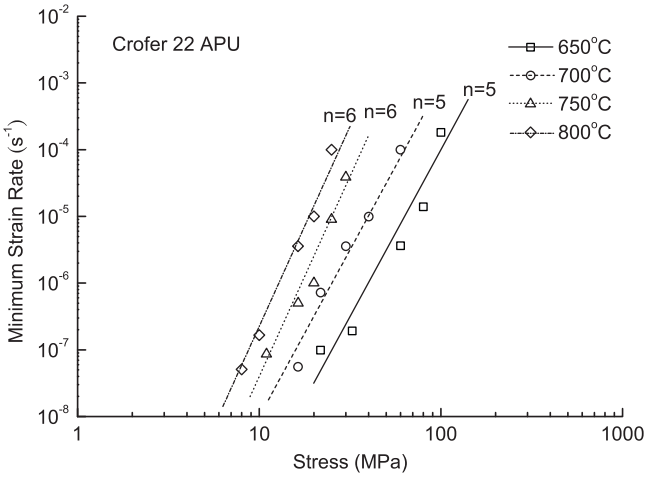

Fig. 7. Relationship between minimum creep strain rate and applied stress for Crofer 22 APU steel at various temperatures.

The effect of temperature on the minimum creep rate for the given steel can be characterized by the following Arrhenius type of equation [29]:

$$\dot{\varepsilon}_{\min} = A \exp\left(\frac{-Q}{RT}\right) \tag{3}$$

where the coefficient A depends mainly on material and stress, Q is the apparent activation energy, R is the universal gas constant, T is the absolute temperature. The value of Q for creep mechanism is ideally a constant for a given material, but may change if the physical mechanism is changed due to a sufficient shift in temperature or stress [28]. In Eq. (3), the value of Q can be determined from the slope of the fitted straight line, by plotting the minimum creep rate as a function of reciprocal temperature in logarithm scale at a given stress (Fig. 8). The apparent activation energy for the given steel at selected stresses (16.4–30 MPa) has a value in the range from 362 to 438 kJ mol^{-1}, as shown in Fig. 8. Although these values have a certain extent of scattering, they are still close to the average value of 393 kJ mol^{-1}. The scattering of Q value may be caused by various creep mechanisms at each given stress or by a limited number of data used for curve fitting. In the present study, the small extent of scattering in the Q value at various stress levels is presumably attributed to the latter, as the creep mechanism was identified as

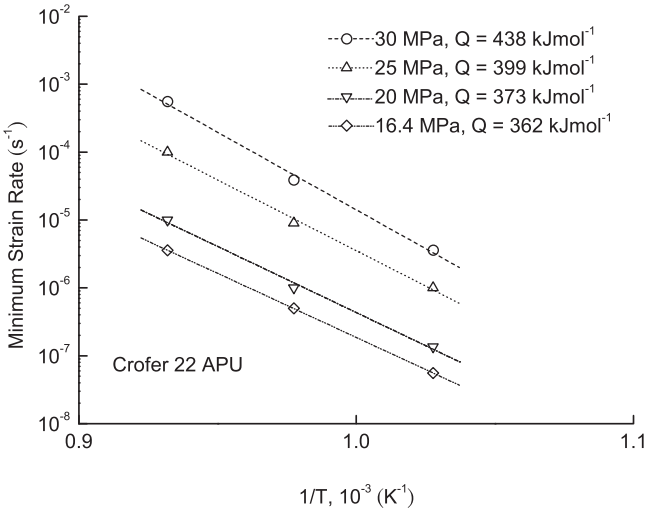

Fig. 8. Minimum strain rates for Crofer 22 APU steel at various temperatures under selected stresses.

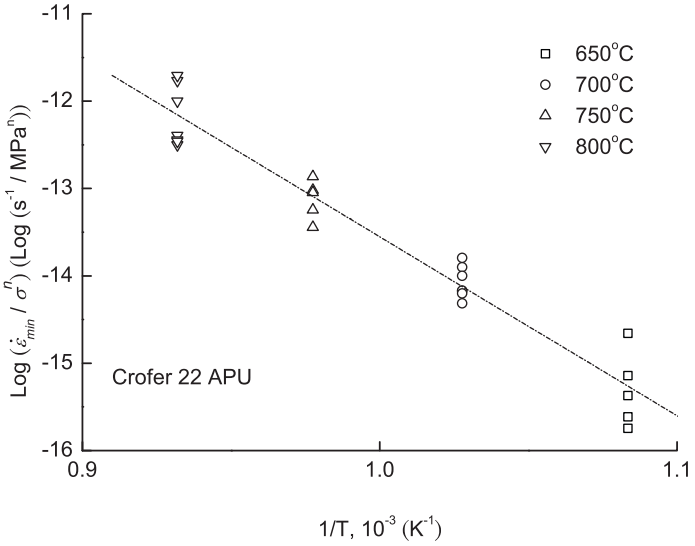

Fig. 9. Minimum strain rates for Crofer 22 APU steel at various temperatures for all the given stresses.

a similar power-law dislocation mechanism at the given temperatures. Note that the four straight lines in Fig. 8 look parallel to one another indicating they have a very close slope (Q value).

Another Arrhenius type of equation is used to describe the creep rate of crystalline alloys. Such an equation describing stress (σ) and temperature (T) dependence of minimum creep rate ($\dot{\varepsilon}_{\min}$) was also applied to determine the activation energy of creep mechanism for the given steel. This equation is given as below [28]:

$$\dot{\varepsilon}_{\min} = A_1 \sigma^n \exp\left(\frac{-Q}{RT}\right) \tag{4}$$

where $\dot{\varepsilon}_{\min}$ has a unit of s^{-1} and A_1 is a constant. The value of Q in Eq. (4) can be determined from the slope of the fitted straight line, by plotting logarithm of the product of minimum creep rate and reciprocal stress with an exponent of n versus logarithm of the reciprocal temperature for all the given stresses, as shown in Fig. 9. Accordingly, the apparent activation energy for all the data points shown in Fig. 9 was determined as 393 kJ mol^{-1}. This value for all the given stress levels is equal to the average value (393 kJ mol^{-1}) determined by four selected stress levels in Fig. 8. Apparently, both approaches (Eqs. (3) and (4)) gave the apparent activation energy Q a value around 393 kJ mol^{-1} for the creep behavior of the Crofer 22 APU stainless steel at 650–800 °C. A dislocation creep mechanism involving climb of dislocations can be diffusion-controlled. This has been evidenced that the apparent activation energy Q for dislocation creep generally agrees with that for lattice self-diffusion [28]. It has been reported that the activation energy for lattice self-diffusion in ferritic steels is commonly in the range of 300–400 kJ mol^{-1} [29]. Therefore, it is suggested that a diffusion-controlled dislocation creep mechanism was involved in the creep behavior of the Crofer 22 APU stainless steel at 650–800 °C.

3.3. Creep lifetime analysis

Monkman and Grant [30] showed that the time to rupture (t_r) in long-term creep tests was inversely proportional to a power function of the minimum creep rate ($\dot{\varepsilon}_{\min}$). The relation can be described as follows:

$$\dot{\varepsilon}_{\min}(t_r)^m = C_{\mathrm{MG}} \tag{5}$$

where C_{MG} is the Monkman–Grant constant which depends on material and temperature. The value of m is commonly in the range of 0.8–1.2 [31]. It implies that the rupture strain is dominated by

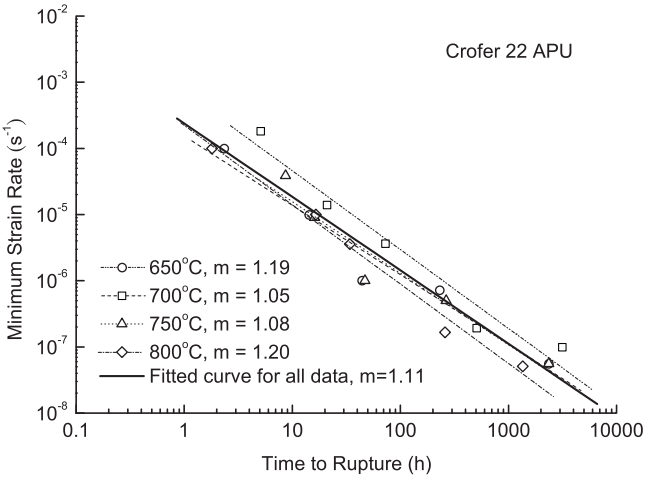

Fig. 10. Monkman–Grant curves of Crofer 22 APU steel at differently given temperatures.

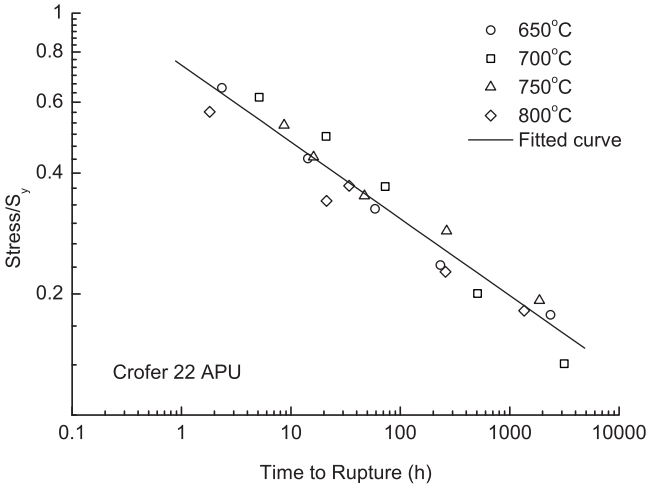

Fig. 12. Normalized stress with respect to yield strength versus rupture time for Crofer 22 APU steel at various temperatures.

the secondary creep for m equal to 1. The relationship is established to determine the value of C_{MG} from short-term tests and the lifetime of a long-term case can be estimated when the minimum creep strain rate is determined. Fig. 10 shows the Monkman–Grant curves of the Crofer 22 APU steel at all the given temperatures. As seen in Fig. 10, the values of m for all conditions are close to 1. It is thus suggested that the secondary creep dominated the rupture strain of the given steel. In addition to fitting the data at each temperature, the entire set of data of all the given temperatures were also fitted to a single straight line according to Eq. (5), as indicated by the solid line in Fig. 10. As a consequence, the Monkman–Grant relation for the given material is expressed as follows:

$$\dot{\varepsilon}_{\min}(t_r)^{1.11} = 2.39 \times 10^{-4}, \quad r^2 = 0.93 \tag{6}$$

where $\dot{\varepsilon}_{\min}$ has a unit of s^{-1}, t_r has a unit of h, and r is the correlation coefficient for the fitted curve of all data. In this regard, Eq. (6) can be applied to predict the creep life of a pSOFC interconnect made of this steel, as the experimental data show an excellent agreement with the Monkman–Grant relation.

In addition to the Monkman–Grant relation, the variation of creep rupture time with applied stress for the Crofer 22 APU steel at various temperatures was also correlated by a simple-power-law relation, as shown in Fig. 11. Creep resistance for such a steel is decreased with an increase in temperature, as shown in Fig. 11. The

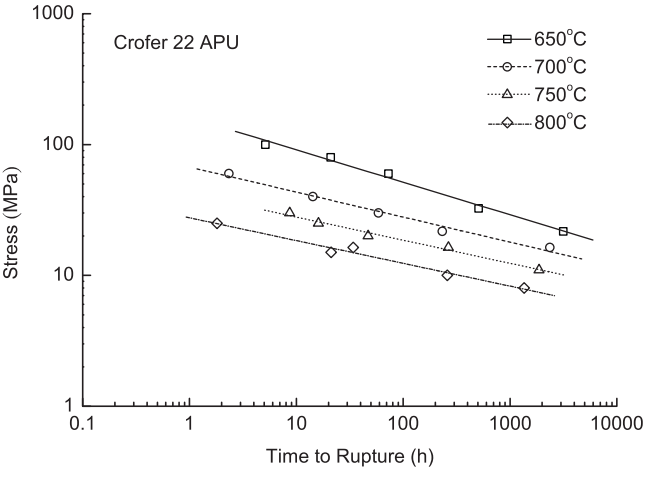

Fig. 11. Applied stress versus rupture time for Crofer 22 APU steel at various temperatures.

relation between creep rupture time and applied stress at a given temperature generally follows a simple power law. The fitted equations and correlation coefficients at the specified temperatures in Fig. 11 are given as follows:

$$650\,^{\circ}\text{C}: \quad \sigma t_r^{0.25} = 162, \quad r^2 = 0.99 \tag{7}$$

$$700\,^{\circ}\text{C}: \quad \sigma t_r^{0.19} = 67.1, \quad r^2 = 0.98 \tag{8}$$

$$750\,^{\circ}\text{C}: \quad \sigma t_r^{0.18} = 42.1, \quad r^2 = 0.99 \tag{9}$$

$$800\,^{\circ}\text{C}: \quad \sigma t_r^{0.17} = 27.5, \quad r^2 = 0.98 \tag{10}$$

where σ is in unit of MPa and t_r is in unit of h. These high values of correlation coefficient indicate that the creep rupture time for the given steel can be predicted through these power-law relations. In order to account for the temperature effect, the applied stress was normalized by yield strength (S_y) of the corresponding temperature. The results in Fig. 11 were re-plotted by representing the normalized stress as a function of rupture time, as shown in Fig. 12. It is seen that the distinctly distanced data points in Fig. 11 became quite closer through such a normalization approach, as shown in Fig. 12. In other words, the intrinsic temperature dependence of rupture time is implied in the yield strength term. The data points shown in Fig. 12 could be well correlated by the following simple power law:

$$\left(\frac{\sigma}{S_y}\right) t_r^{0.20} = 0.75, \quad r^2 = 0.95 \tag{11}$$

where σ has a unit of MPa and t_r is in unit of h. Therefore, the creep rupture time of Crofer 22 APU can be estimated through the universal relation given in Eq. (11) once the applied stress is known.

Another well-known creep life relationship was also applied in this study to correlate the creep rupture time with applied stress and temperature. This relationship is called Larson–Miller relationship. Larson and Miller [28] assumed the following relation between creep rupture time, applied stress and temperature:

$$P_{LM} = T(\log t_r + C) \tag{12}$$

where P_{LM} is the Larson–Miller parameter with a function of applied stress, T is temperature in Kelvin scale, and t_r is in unit of h. The value of C can be determined by extrapolating an intercept of $\log t_r = -C$ on a plot of $\log t_r$ versus $1/T$ at $1/T = 0$. Accordingly, the values of C at selected stresses in the given temperatures for Crofer 22 APU were determined as 13.1–25.6. Values of C for steels and other engineering metals are often around 20 [32]. In the present work, an average value of 18.7 was chosen for the constant C in Eq. (12).

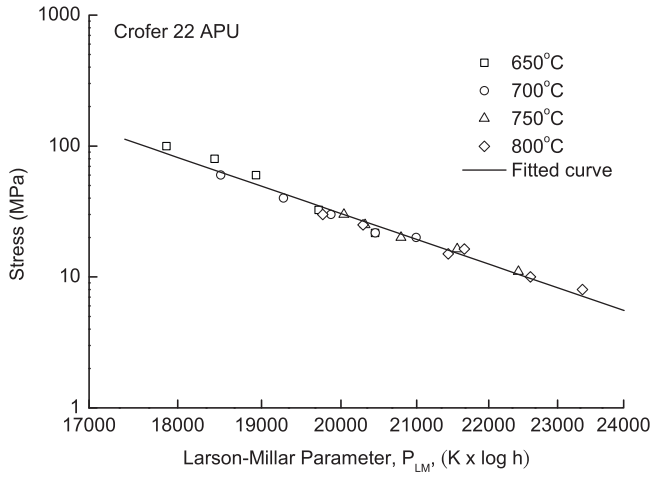

Fig. 13. Master curve of Larson–Miller parameter for Crofer 22 APU steel.

Once the value of C is known, values of P_{LM} determined by Eq. (12) can be plotted against stress, as shown in Fig. 13. As shown in Fig. 13, the Larson–Miller parameter and applied stress could be well correlated by a simple power law for the given steel at various temperatures. The fitted master curve of the Larson–Miller parameter for Crofer 22 APU is given as follows:

$$\sigma = 4.96 \times 10^{41} P_{LM}^{-9.35}, \quad r^2 = 0.98 \tag{13}$$

where σ is in unit of MPa. The test data used to make the plot of P_{LM} versus applied stress generally involve rupture times shorter than the service lives of interest. This means the test data at short t_r and high temperatures are readily used to predict the creep behavior at longer t_r and lower temperatures. In this regard, Eqs. (12) and (13) can be combined to assess the creep lifetime of pSOFC interconnects made of Crofer 22 APU at various combinations of stress and temperature.

3.4. Fractography analysis

Features of the fracture surface and microstructure in the Crofer 22 APU specimens after creep test at 650–800 °C look similar, presumably due to a similar power-law dislocation creep mechanism. Representative SEM micrographs of the fracture surface are shown in Fig. 14. After a significant extent of necking in the tertiary creep region, the fractured cross-section was reduced to a very small area, as shown in Fig. 14(a). A ductile fracture pattern was identified by the dimpled features shown in Fig. 14(b). A SEM micrograph of the Crofer 22 APU microstructure before tensile or creep test is shown in Fig. 15. The micrograph in Fig. 15 shows clear ferritic grain boundaries without cavities. The average grain size is about 45 μm. As grain size decreases, the surface area to volume ratio of the grain increases, allowing more pile-ups of dislocations at a grain boundary [33]. Since it requires more energy to move dislocations to another grain during a tensile test, these dislocations pile up along the boundary and increase the yield strength of the steel. Additionally, although it is essentially assumed that the power-law creep is independent of grain size, steady-state creep rate for pure metals and alloys is only independent of grain size for grain size greater than 100 μm [34]. It has been experimentally observed that the steady-state creep rate would increase with a decrease in grain size for smaller grains [34]. As only one size of microstructure is investigated in the current work, a further study with other grain sizes is needed to investigate the effects of grain size on tensile and creep properties for the Crofer 22 APU steel.

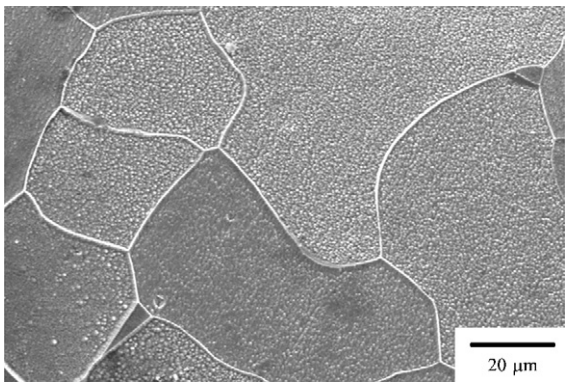

Fig. 15. SEM micrograph of microstructure in the Crofer 22 APU specimen before creep test.

Representative SEM micrographs of the Crofer 22 APU microstructure after creep test at 700 °C under different stresses are shown in Fig. 16. In comparison with the micrograph in Fig. 15, substantial cavities were found, particularly at grain boundaries, as shown in Fig. 16. These cavities can be classified into three types, C1, C2, and C3, by their location, as shown in Fig. 16. Cavities of type C1 are distributed almost within the grains and related to the tetragonal precipitates. TiN can be nucleated and precipitated by means of externally applied force in terms of the theory of kinetics [35]. As described above, tetragonal precipitates of TiN were found in the tensile specimens after a short-term tensile test at 700 °C and above (Fig. 5). Therefore, the tetragonal precipitates of TiN are presumably formed at the early stage of creep test with the help of creep loading as a driving force for precipitation. It has been found that fine TiN precipitates can disturb the dislocation movement by pinning the dislocations and/or incorporate the bow-type moving dislocations [36]. Therefore, the interaction between the TiN precipitates and the dislocations could decrease the creep rate and increase the high-temperature creep strength for the Crofer 22 APU steel. In addition, round cavities of types C2 and C3 were mostly formed at triple grain junctions and grain boundaries, respectively. It has been

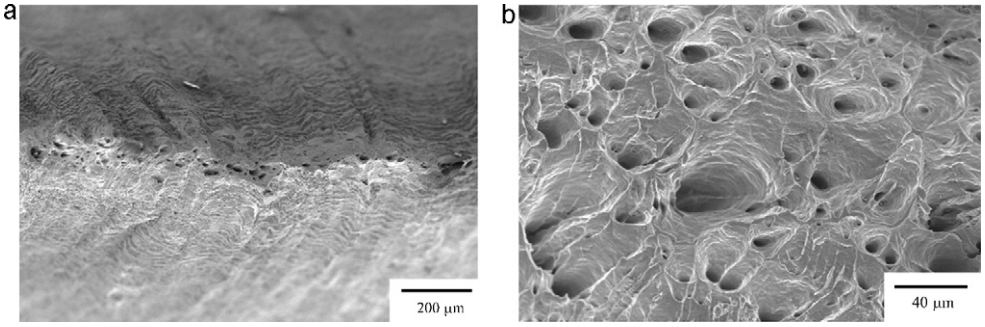

Fig. 14. Fractograph of a Crofer 22 APU specimen after creep test at 700 °C: (a) low magnification; (b) high magnification.

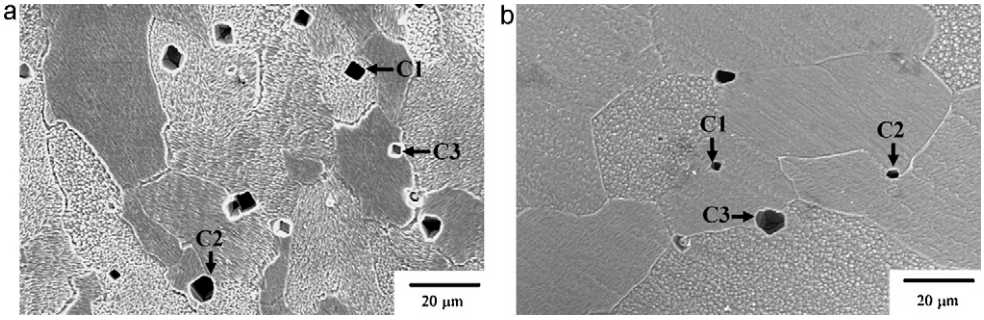

Fig. 16. SEM micrographs of microstructure in the Crofer 22 APU steel after creep test at 700 °C under differently applied stresses: (a) 60 MPa; (b) 16.4 MPa.

reported that creep cavities are usually nucleated at grain boundaries, where high stress concentrations could develop [37]. These high stress-concentration sites include triple grain junctions and hard particles at grain boundaries [37]. Such a phenomenon was clearly observed in the Crofer 22 APU steel subjected to a creep loading, as shown in Fig. 16. In addition, it was also found that a greater amount of creep cavities were formed under a greater applied stress, as shown in Fig. 16(a). A previous analysis [38] has shown that stress concentrations indeed developed at triple grain junctions in gamma iron or stainless steel under a power-law creep condition. Therefore, a greater applied stress apparently provided a larger driving force for nucleation and coalescence of creep cavities leading to a shorter rupture time for the cases studied in the present work.

4. Conclusions

1. The variation of yield strength with temperature for Crofer 22 APU can be described by a sigmoidal relation. The yield strength is gradually decreased with an increase in temperature up to about 500 °C. The high temperature softening effect dominates the mechanical behavior between 500 and 700 °C, as the yield strength is considerably decreased with increasing temperature. The gradual reduction of yield strength with increasing temperature at temperature above 700 °C is attributed to a dynamic precipitation strengthening effect.
2. A diffusion-controlled dislocation creep mechanism is involved in the power-law creep behavior of the Crofer 22 APU stainless steel at 650–800 °C, according to the values of creep stress exponent and activation energy.
3. Creep rupture time of the Crofer 22 APU stainless steel can be well described by the Monkman–Grant and Larson–Miller relations. A universal simple-power-law relation between creep rupture time and normalized stress is proposed to cover all of the given testing conditions.
4. A ductile, dimpled fracture pattern with considerable necking is identified for the Crofer 22 APU specimens after creep test. Tetragonal cavities within grains are formed at precipitates during creep test. Creep cavities are mostly formed at grain boundaries and triple grain junctions due to high stress concentrations. More cavities are found in the specimens subjected to a greater applied creep stress, presumably due to a larger driving force for cavity formation.

Acknowledgement

This work was supported by the National Science Council (Taiwan) under Contract No. NSC 99-2221-E-008-012-MY3.

References

[1] A. Weber, E. Ivers-Tiffée, J. Power Sources 127 (2004) 273–283.
[2] W.Z. Zhu, S.C. Deevi, Mater. Sci. Eng. 348 (2003) 227–243.
[3] J.H. Zhu, Y. Zhang, A. Basu, Z.G. Lu, M. Paranthaman, D.F. Lee, E.A. Payzant, Surf. Coat. Technol. 177–178 (2004) 65–72.
[4] H. Kurokawa, K. Kawamura, T. Maruyama, Sol. Stat. Ion 168 (2004) 13–21.
[5] G. Cabouro, G. Caboche, S. Chevalier, P. Piccardo, J. Power Sources 156 (2006) 39–44.
[6] I. Antepara, I. Villarreal, L.M. Rodriguez-Martinez, N. Lecanda, U. Castro, A. Laresgoiti, J. Power Sources 151 (2005) 103–107.
[7] J.W. Fergus, Mater. Sci. Eng. 397 (2005) 271–283.
[8] W.J. Quadakkers, J. Piron-Abellan, V. Shemet, L. Singheiser, Mater. High Temp. 20 (2003) 115–127.
[9] K. Huang, P. Hou, J. Goodenough, Sol. Stat. Ion 129 (2000) 237–250.
[10] T. Horita, Y. Xiong, H. Kishimoto, K. Yamaji, N. Sakai, H. Yokokawa, J. Power Sources 131 (2004) 293–298.
[11] J. Froitzheim, G.H. Meier, L. Niewolak, P.J. Ennis, H. Hattendorf, L. Singheiser, W.J. Quadakkers, J. Power Sources 178 (2008) 163–173.
[12] P. Lamp, J. Tachtler, O. Finkenwirth, S. Mukerjee, S. Shaffer, Fuel Cells 3 (2003) 146–152.
[13] C.-K. Lin, T.-T. Chen, Y.-P. Chyou, L.-K. Chiang, J. Power Sources 164 (2007) 238–251.
[14] C.-K. Lin, L.-H. Huang, L.-K. Chiang, Y.-P. Chyou, J. Power Sources 192 (2009) 515–524.
[15] Z. Yang, G.-G. Xia, M.S. Walker1, C.-M. Wang, J.W. Stevenson, P. Singh, Int. J. Hydrogen Energy 32 (2007) 3770–3777.
[16] S.J. Geng, J.H. Zhu, Z.G. Lu, Sol. Stat. Ion 177 (2006) 559–568.
[17] P.E. Gannon, C.T. Tripp, A.K. Knospe, C.V. Ramana, M. Deibert, R.J. Smith, V.I. Gorokhovsky, V. Shutthanandan, D. Gelles, Surf. Coat. Technol. 188–189 (2004) 55–61.
[18] S. Fontana, R. Amendola, S. Chevalier, P. Piccardo, G. Caboche, M. Viviani, R. Molins, M. Sennour, J. Power Sources 171 (2007) 652–662.
[19] ASTM Standard E8/E8M-08, Standard Test Method for Tension Testing of Metallic Materials, Annual Book of ASTM Standards, ASTM International, West Conshohohocken, PA, USA, 2008, pp. 1–25.
[20] T.R. McNelly, S.F. Gates, Acta Metall. 26 (1978) 1605–1614.
[21] L.P. Kubin, K. Chihab, Y. Estrin, Acta Metall. 36 (1988) 2707–2718.
[22] J. Chen, B. Young, B. Uy, J. Struct. Eng. 132 (2006) 1948–1954.
[23] J. Chen, B. Young, J. Constr. Steel Res. 64 (2008) 689–703.
[24] J.D. Baird, A. Jamieson, J. Iron Steel Inst. 204 (1966) 793–803.
[25] N. Fujita, K. Ohmura, M. Kikuchi, T. Suzuki, S. Funai, I. Hiroshige, Scr. Mater. 35 (1996) 705–710.
[26] H. Yan, H. Bi, X. Li, Z. Xu, Mater. Charact. 60 (2009) 204–209.
[27] A.K. Mukherjee, J.E. Bird, J.E. Dorn, Trans. Am. Soc. Metals 62 (1969) 155–179.
[28] N.E. Dowling, Mechanical Behavior of Materials, 3rd ed., Pearson Education, Inc., New Jersey, USA, 2007, pp. 779–797.
[29] K. Maruyama, H. Ghassemi Armaki, R.P. Chen, K. Yoshimi, M. Yoshizawa, M. Igarashi, Int. J. Pressure Vessels Piping 87 (2010) 276–281.
[30] F.C. Monkman, N.J. Grant, Proc. ASTM 56 (1956) 593–620.
[31] P.J. Ennis, A. Czyrska-Filemonowicz, Oper. Maint. Mater. 1 (2002) 1–28.
[32] M.E. Kassner, T.A. Hayes, Int. J. Plast. 19 (2003) 1715–1748.
[33] J.W. Morris, in: S. Takaki, T. Maki (Eds.), Proceedings, International Symposium on Ultrafine Grained Steels, Iron and Steel Inst. Japan, Tokyo, 2001, pp. 34–41.
[34] C.R. Barrett, J.L. Lytton, O.D. Sherby, Trans. AIME 239 (1967) 170–180.
[35] X.-F Shi, G. -G. Cheng, Steelmak 24 (2008) 36–39.
[36] D.-S. Bae, M.-H. Hong, K. Miyahara, Sol. Stat. Commun. 125 (2003) 347–350.
[37] M.H. Yoo, H. Trinkaus, Metall. Trans. 14A (1983) 547–561.
[38] A.S. Argon, I.-W. Chen, C.-W. Lau, Met. Soc. AIME (1980) 46–85.